Plasma reforming of naphthalene as a tar model compound of biomass gasification

Yaoling Wang[1], Haiping Yang[2], Xin Tu[1*]

[1] Department of Electrical Engineering and Electronics, University of Liverpool, L69 3GJ, Liverpool, United Kingdom

[2] State Key Laboratory of Coal Combustion, School of Energy and Power Engineering, Huazhong University of Science and Technology, 430074 Wuhan, China

*Corresponding author (Dr. X. Tu)

Email address: xin.tu@liverpool.ac.uk;

Accepted by Energy Conversion and Management

Abstract

The contamination of producer gas with tars from biomass gasification remains a significant challenge in the bioenergy industry and a critical barrier, limiting the commercial applications of biomass gasification. Non-thermal and non-equilibrium plasma offers an unconventional and emerging technology for the effective reduction of problematic tars from gasification. In this study, we investigated plasma reforming of naphthalene as a two-ring tar model compound using a gliding arc discharge (GAD) reactor with/without steam. The influence on the plasma conversion of naphthalene based on the inlet naphthalene concentration, discharge power and steam-to-carbon ratio was examined to understand the effects of these operating parameters on the destruction of tar, gas selectivity/yield and process efficiency. Adding H_2O in the plasma process generates oxidative OH radicals, creating additional reaction routes for the step-wised oxidation of naphthalene and its fragments towards the CO, CO_2 and water. The optimum ratio (2.0) of steam-to-carbon was identified to achieve the highest naphthalene conversion (84.8%), C_2H_2 yield (33%), total gas yield (72.2%) and energy efficiency (5.7 g/kWh). The effect of the amount of steam on the plasma reduction of tars was dependent on the balance between two opposite effects due to the presence of steam: positive effect of OH radicals and the negative effect of electron attachment on water molecules. Introducing an appropriate amount of steam to the plasma reduction of naphthalene also substantially minimized the formation of by-products and enhanced the carbon balance. Plausible reaction mechanisms for the plasma decomposition of naphthalene were proposed through a comprehensive analysis of gaseous and condensable products combined with plasma spectroscopic diagnostics.

Keywords: Non-thermal plasma; Steam reforming; Naphthalene; Tar; Biomass gasification

1. Introduction

Biomass has been highlighted as one of the most important renewable energy sources to meet the increasing energy demand as well as the mitigation of global climate change. Biomass gasification provides a green and sustainable route for the production of high calorific value biosyngas (H_2 and CO), which can be used to produce electricity, heat, chemicals and fuels [1]. However, biosyngas generated from biomass gasification processes contains undesirable contaminates, including particulate matters, SO_2, NO_x and tars. Particularly, the contamination of biosyngas with problematic tars has been highlighted as one of the major challenges in the bioenergy industry and a critical barrier that limits the commercial applications of biomass gasification technology. Gasification tar, as a mixture of complex condensable hydrocarbons, consists of a range of aromatic hydrocarbons with single to multiple rings [2]. The presence of tars in biosyngas reduces the quality of producer gas and causes serious operational issues such as blocking, fouling and corrosion throughout the process [3]. Hence, developing cost-effective and emerging processes for the reduction of problematic tars in biomass gasification to produce high-quality and clean biosyngas is essential and of vital importance for the successful implementation of gasification technology, especially when using syngas for the further synthesis of higher value chemical feedstocks.

Considerable efforts have been placed on finding solutions for the reduction of tars from the gasification of biomass waste, including physical methods (e.g. using cyclone, bag filters, and absorbers) [2, 4], thermal cracking [5] and catalytic reforming [6-8]. However, the use of physical methods can lead to secondary pollution especially when removing high

concentration tars with multiple aromatic rings. In addition, using a physical approach cannot recover the chemical energy contained in tars, thus lowering the overall energy efficiency of this technology [3]. Thermal cracking processes usually requires a very high reaction temperature (over 1000 °C) for the complete decomposition of heavy carbon molecules, incurring high energy costs [8]. Although catalytic reforming has been considered as a very attractive process for the conversion of tars into syngas, the major challenge in conventional catalytic reforming of tars is catalyst deactivation and stability resulted from the blocking and poisoning of the catalysts due to carbon deposition on catalyst surfaces at relatively high temperatures (> 600 ^{o}C). Finding highly reactive and stable coke-resistant catalysts is crucial but remains a big challenge for the long-term operation of biomass gasification systems to get high quality biosyngas at commercial scale.

Non-thermal plasma (NTP) has attracted increasing interest as an unconventional but promising and emerging low temperature technology for tar reduction and fuel synthesis [9, 10]. Electrons and reactive species including radicals and excited species generated in NTP can initiate a variety of chemical reactions at ambient conditions. NTP is highly non-equilibrated, which offers its unique capability to enable thermodynamic unfavourable chemical processes (e.g., high temperature reforming reactions) to proceed under ambient conditions[11, 12]. Plasma processes can be switched on and off instantly, thus offering a high flexibility that can be integrated with renewable and clean energy sources such as wind and solar power, especially surplus energy from wind power for chemical energy storage to further reduce carbon emissions.

Despite significant efforts having been concentrated on investigating the destruction of gas pollutants such as volatile organic compounds (VOCs) using different plasma processes, far less has been done on the plasma processing of tars for biosyngas clean-up and energy recovery. Up until now, most of previous studies owing to the complicated structure and composition of tars, have mainly concentrated on the reforming of tar model compounds with a single aromatic ring (e.g. toluene [13-15], benzene [7, 15, 16], phenol [17], etc) while naphthalene, a major substance of tars, has received less attention [18, 19]. Although using NTP for the degradation of highly diluted naphthalene (ppm level) in the form of polycyclic aromatic hydrocarbons (PAHs) was reported, mainly through an oxidation process to produce CO_2 and water. Yu et al. assessed the influence of different carrier gases (Ar, N_2, O_2 and air) on the destruction of naphthalene as a PAH pollutant undergoing combustion using a direct-current (DC) gliding arc discharge (GAD) at ambient pressure [20]. The highest conversion of naphthalene was obtained when using oxygen as a carrier gas [20]. Ayman et al. investigated the oxidation of naphthalene (20-70 ppm) using a carrier gas containing oxygen in a surface discharge reactor, and found that the removal of naphthalene declined dramatically from 100% to 31.2% when changing the gas flow from 2 to 4 L/min [21, 22]. Wu et al. evaluated naphthalene (60 ppm) oxidation over a TiO_2/diatomite catalyst coupled with a dielectric barrier discharge (DBD) [23, 24]. Ozone (150 ppm) was identified as a by-product in the plasma-catalytic oxidation of naphthalene [23, 24]. Clearly, in these reported works naphthalene was usually treated as a model pollutant of PAHs with low concentration (ppm level), whereas the concentration of naphthalene to be removed from the gasification of biomass waste is significantly higher (1-3 orders of magnitude) and the target

products of plasma reforming of naphthalene are syngas with light hydrocarbons, to achieve both tar reduction and energy recovery rather than CO_2, water or ozone. Water vapor or steam is a common product present in the producer gas from biomass gasification. From an industrial application point of view, gas humidity is one of the most critical factors affecting the effectiveness of plasma reforming processes. However, far less has been done to understand how the presence of H_2O and the steam-to-carbon (S/C) ratio affects the conversion of tars (e.g., naphthalene) and by-products formation in the plasma processing of naphthalene. The influence of H_2O on the plasma chemistry and reaction pathways in the plasma reduction of naphthalene is still not clear. Therefore, gaining in-depth understanding on the plasma reforming of naphthalene especially in the presence of steam is the key to make this promising technology more attractive and competitive. In addition, a comprehensive analysis of gaseous products and by-products coupled with plasma optical diagnostics could lay an important foundation to gain new insights into the underlying reforming chemistry and reaction pathways in this process, which could generate valuable information to further enhance and optimize the plasma tar reduction technology.

In this work, plasma reforming of naphthalene with and without steam was performed using a gliding arc system with knife-shaped electrodes. Gliding arc discharge has proved to be more efficient for the conversion of methane, carbon dioxide and large carbonic molecules, especially aromatic compounds (e.g., toluene), compared to other plasma technologies, such as corona discharge, glow discharge and DBD. Naphthalene was selected as a tar surrogate as it represents the stable two-ring aromatic products formed in biomass gasification but has not

received sufficient attention in the past years. The influence of various operating parameters such as the concentration of the naphthalene feed, S/C ratio and discharge power were examined. In addition, plasma spectroscopic diagnostics was used to investigate the generation of chemically reactive species (e.g. OH, C_2, CN and NH) and their roles in the plasma tar reduction process. Underlying plasma chemistry and plausible reaction pathways in the plasma reforming of naphthalene were discussed, through a comprehensive analysis of the gaseous and condensable liquid products coupled with plasma spectroscopic diagnostics.

2. Experimental

2.1 Experimental system and product analysis

The experiment was performed in a GAD reactor equipped with two semi-ellipsoidal metal electrodes (stainless steel), as shown in Fig. 1. The shortest discharge gap was fixed at 2 mm. A gas nozzle was placed between the electrodes and the diameter of the nozzle exit was 1.5 mm. Naphthalene powders were placed in a metal vessel and vaporized at 60-75 ^{o}C using a water bath. A mixture of naphthalene and nitrogen with or without steam was heated up to 200 ^{o}C before being injected into the GAD reactor. The flow rate of nitrogen was maintained at 4 L/min and the concentration of naphthalene can be controlled at 1.1-2 mg/L by changing the temperature of the water bath (60-75 ^{o}C). To understand the effect of steam on the reduction of naphthalene, the molar ratio of steam-to-carbon could be changed from 0.5 to 4. The GAD reactor was powered by a 10 kV/50 Hz neon transformer. The electrical signals (arc voltage U and arc current I) were sampled by a Tektronix digital oscilloscope (MDO3024).

The gas products were measured by an Agilent 7820A gas chromatography system equipped with a flame ionization detector (FID) and a thermal conductivity detector (TCD). A Molecular Sieve 5A (60-80 mesh) column (HP MOLESIEVE) was used for the separation of H_2 and CO, while a HP-PLOT/Q column was used for the measurement of CO_2, CH_4 and C_2-C_4 hydrocarbons. The GC was calibrated for each gas with a wide range of concentrations using standard calibration gas mixtures. The condensable liquid products in the effluent were dissolved in dichloromethane (DCM) through an ice trap. The liquid samples were collected and analyzed using gas chromatography – mass spectrometry (GC-MS, Agilent GC7820A, MSD) containing a HP-5MS column and qualitatively identified using a standard database of the National Institute of Standards and Technology (NIST). The GC-MS was calibrated for naphthalene using different naphthalene concentrations. The optical emission spectra of the GAD with and without steam was measured by a Princeton Instrument triple-grating spectrometer (Model320) equipped with an ICCD camera.

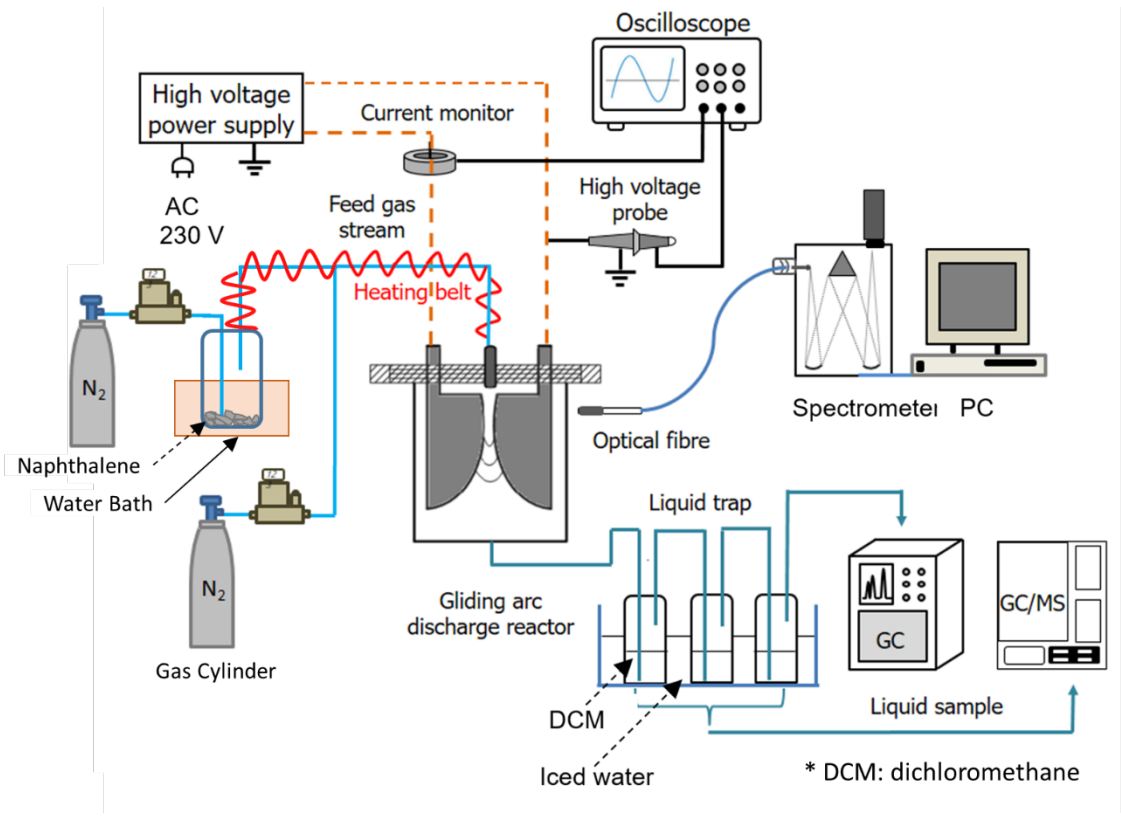

Fig. 1 Schematic of the experimental system.

2.2 Definition of parameters

In the plasma processing of naphthalene, the conversion of naphthalene is defined as:

$$X_{C_{10}H_8}(\%) = \frac{C_i - C_o}{C_i} \times 100\% \tag{1}$$

Where C_i is the inlet concentration of naphthalene and C_o is the concentration of naphthalene after the plasma reaction.

The yield of gaseous products (CO_2, CO, C_xH_y and H_2) is calculated as:

$$Y_{CO_x}(\%) = \frac{CO_x \text{ produced } (mol/s)}{10 \times C_{10}H_8 \text{ input } (mol/s)} \times 100\% \quad (x = 1 \text{ and } 2) \tag{2}$$

$$Y_{C_xH_y}(\%) = \frac{x \times C_xH_y \text{ produced } (mol/s)}{10 \times C_{10}H_8 \text{ input } (mol/s)} \times 100\% \tag{3}$$

Without steam

$$Y_{H_2}(\%) = \frac{H_2 \text{ produced}(\text{mol/s})}{4 \times C_{10}H_8 \text{ input } (\text{mol/s})} \times 100\ \% \tag{4}$$

With steam

$$Y_{H_2}(\%) = \frac{H_2 \text{ produced}(\text{mol/s})}{4 \times C_{10}H_8 \text{ input } (\text{mol/s}) + H_2O \text{ input}(\text{mol/s})} \times 100\ \% \tag{5}$$

The selectivity of CO_x (x = 1 and 2) is defined as:

$$S_{CO_x}(\%) = \frac{\sum Y_{CO_x}(x=1,2)(\%)}{X_{C_{10}H_8}(\%)} \times 100\% \tag{6}$$

The selectivity of hydrocarbons (C_xH_{2x+2}, C_xH_{2x}, C_xH_{2x-2}, or C_1-C_4) is defined as:

$$S_{C_xH_{2x+2}}(\%) = \frac{\sum Y_{C_xH_{2x+2}}(x=1,2,3,4)(\%)}{X_{C_{10}H_8}(\%)} \times 100\% \tag{7}$$

$$S_{C_xH_{2x}}(\%) = \frac{\sum Y_{C_xH_{2x}}(x=2,3,4)(\%)}{X_{C_{10}H_8}(\%)} \times 100\% \tag{8}$$

$$S_{C_xH_{2x-2}}(\%) = \frac{\sum Y_{C_xH_{2x-2}}(x=2)(\%)}{X_{C_{10}H_8}(\%)} \times 100\% \tag{9}$$

$$S_{C_xH_y}(\%) = \frac{\sum Y_{C_xH_y}(x=1,2,3,4)(\%)}{X_{C_{10}H_8}(\%)} \times 100\% \tag{10}$$

$$\text{Selectivity of } C_1 \text{ - } C_4(\%) = \frac{S_{C_xH_y}}{\sum S_{C_xH_y}}(x=1,2,3,4) \times 100\% \tag{11}$$

The carbon balance of the plasma tar reforming is given by:

Without steam

$$\text{Carbon balance}(\%) = 100\% - \sum S_{C_xH_y}(x=1,2,3,4)\ (\%) \tag{12}$$

With steam

$$\text{Carbon balance}(\%)=100\% - \sum S_{C_xH_y}\,(x=1,2,3,4)\ (\%) - S_{CO_x} \tag{13}$$

The discharge power P is determined by [25]:

$$P(W)=\frac{1}{T}\int_0^{t=T} U(t)\times I(t)\,dt \tag{14}$$

The energy efficiency for tar conversion is defined as:

$$E(\text{g/kWh})=\frac{\text{mass of converted tar (g/h)}}{\text{discharg power (kW)}} \tag{15}$$

3. Results and discussion

3.1 Plasma processing of naphthalene without steam

3.1.1 Effect of discharge power

Fig. 2(a) illustrates the influence of plasma power on the destruction of naphthalene at a fixed $C_{10}H_8$ concentration. Clearly, increasing discharge power from 32 to 77 W slightly enhanced the conversion of naphthalene from 66.0% to 70.8% with the conversion being almost constant when the power was higher than 57 W, as plotted in Fig. 2(a). Furthermore, carbon balance reached a maximum (53.0%) at 46 W, and then dropped almost linearly when further increasing the plasma power as more carbon deposition could be expected at a higher power. The yields of gaseous hydrocarbons also increased with the rising discharge power, especially for C_2H_2, a major hydrocarbon produced in this process. Higher power input generated more C_2H_2 in the plasma reforming of naphthalene. Note that the yield of hydrogen was negligible

and thus was not presented.

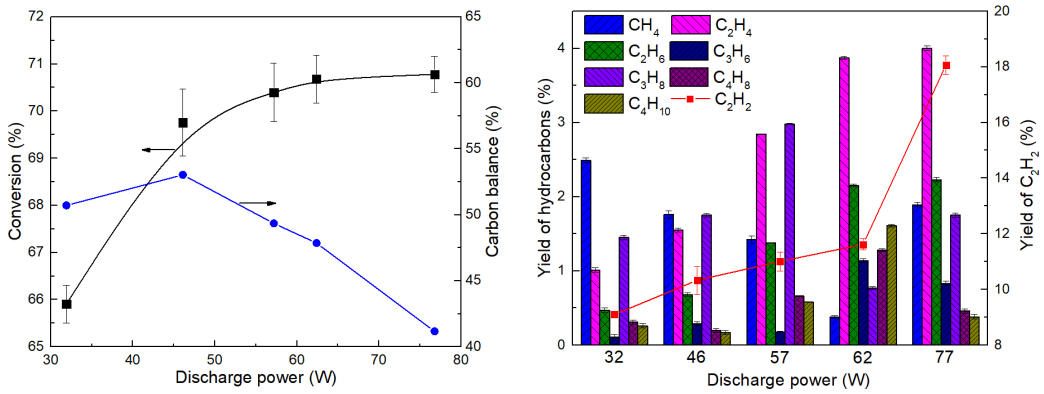

(a) (b)

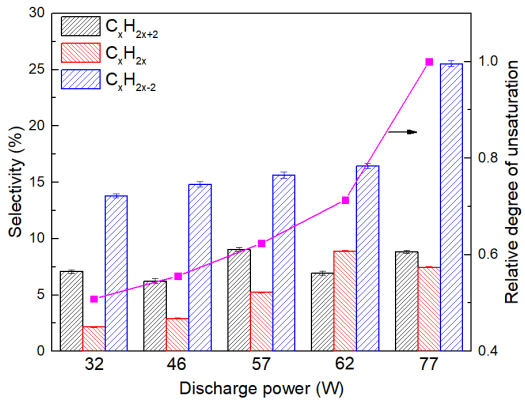

(c)

Fig. 2 Influence of plasma power on (a) $C_{10}H_8$ conversion, (b) yield of gaseous products, (c) selectivity of hydrocarbons with different unsaturation degrees ($C_{10}H_8$ content: 1.7 g/Nm^3).

Fig. 2(c) presents the selectivity of hydrocarbons with different degrees of unsaturation. Unsaturated hydrocarbon alkynes (C_xH_{2x-2}) were the main products in this reaction when compared to alkanes (C_xH_{2x+2}) and alkenes (C_xH_{2x}). It is important to note that the relative degree of unsaturation for hydrocarbons increased with the increase of discharge power, which suggests higher power enhanced dehydrogenation reactions and generated more carbon

deposition. In the plasma reforming of naphthalene without steam, carbon deposition can be found on the electrode surface. Fig. 3(a) shows the scanning electron microscope (SEM) images of the deposited carbon. Interestingly, the major structure of the deposited carbon was the spherical carbon nanoparticles with a particle diameter of 40 - 60 nm. Tu and Whitehead also reported the production of spherical carbon nanoparticles with a diameter of 40-50 nm in the plasma dry reforming of CH_4 and CO_2 (without steam) using a similar gliding arc plasma reactor [26]. In addition, recent works reported the formation of amorphous carbon and its graphitized structure in the plasma reforming of tars using a rotating gliding arc or a microwave plasma [27, 28].

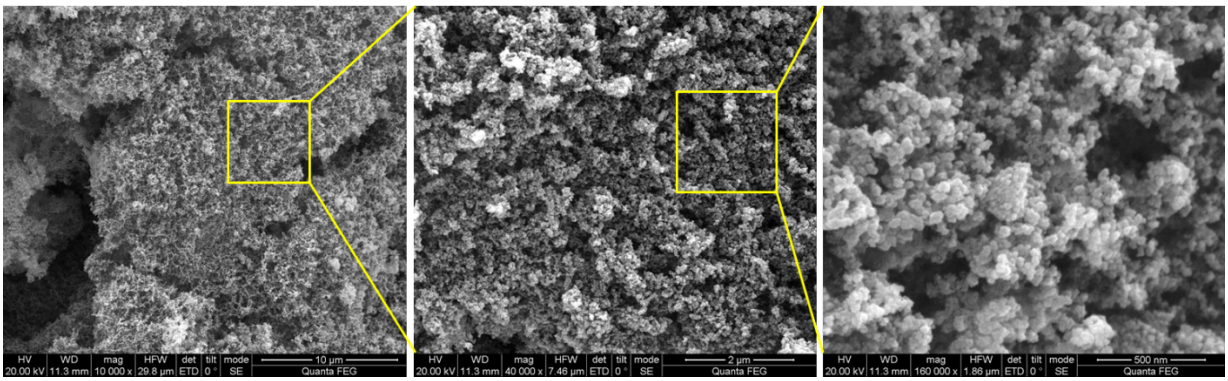

Fig. 3 SEM images of the collected solid carbon deposition. ($C_{10}H_8$ content: 1.7 g/Nm^3, Discharge power: 57 W)

3.1.2 Effect of the initial naphthalene concentration

The initial $C_{10}H_8$ concentration also affects the plasma reforming of naphthalene (Fig. 4). The conversion of naphthalene decreased substantially from 84.7% to 69.7% at a fixed discharge power despite the converted amount of naphthalene increase when the initial concentration of naphthalene was almost doubled from 1.1 to 2.0 mg/L, resulted in the enhancement of the

energy efficiency for $C_{10}H_8$ conversion (from 2.9 to 4.3 g/kWh). These findings suggest that GAD is capable of converting a higher naphthalene feed at the compensation of slightly decreased conversion.

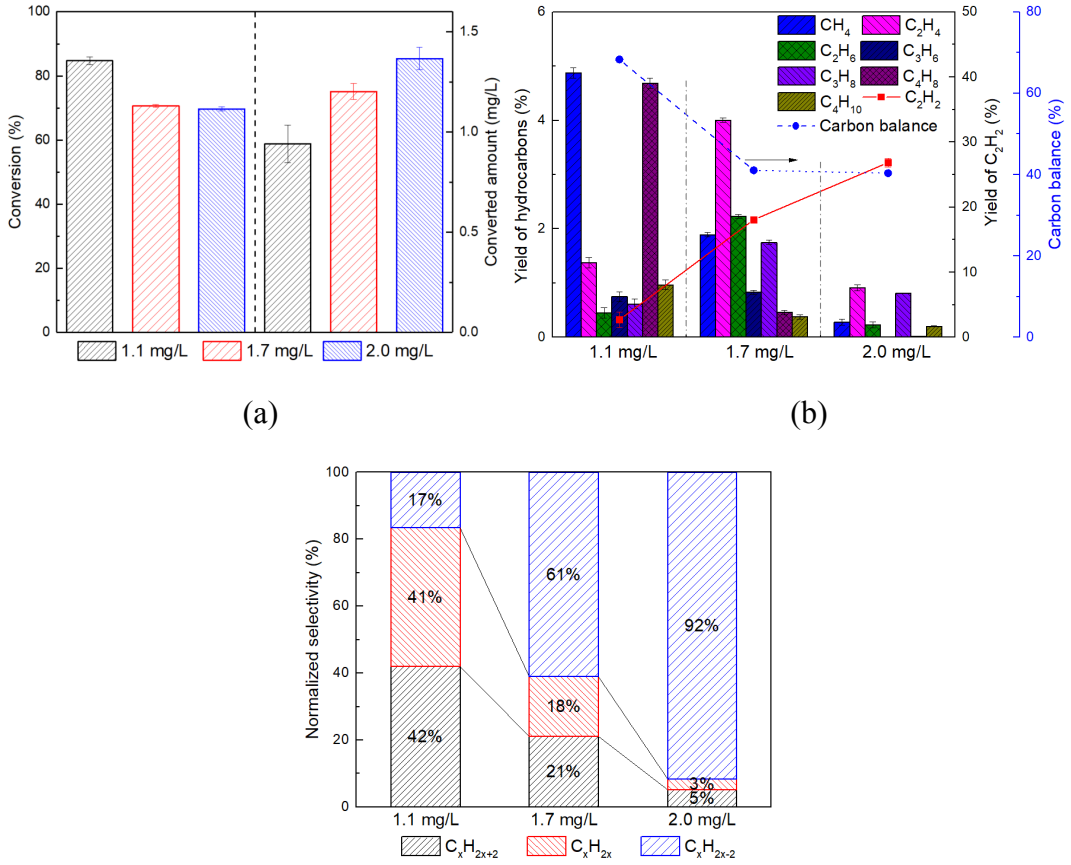

Fig. 4 Influence of initial naphthalene concentration on (a) $C_{10}H_8$ conversion; (b) yield of gaseous products and carbon balance; (c) normalized selectivity of hydrocarbons with different unsaturation degrees (Discharge power: 77 W).

Changing the initial concentration of $C_{10}H_8$ significantly changed the yield of gas products (Fig. 4(b)). For example, the yield of C_2H_2 was increased significantly when increasing the naphthalene feed concentration. In addition, more CH_4 and C_4H_{10} were produced in the

reaction at a low naphthalene concentration of 1.1 mg/L, while higher $C_{10}H_8$ concentration produced less hydrocarbons (except C_2H_2) and more carbon deposition. Additionally, higher $C_{10}H_8$ concentration led to more carbon deposition, which can be evidenced by the declined carbon balance from 68.3% (at 1.1 mg/L) to 40.4% (at 2.0 mg/L), as plotted in Fig. 4(b).

Changing the initial content of $C_{10}H_8$ also significantly changed the normalized selectivity of hydrocarbons. Fig. 4(c) shows the normalized selectivity of C_xH_{2x-2} increased dramatically from 17% to 92%, while the selectivity of C_xH_{2x} and C_xH_{2x+2} was significantly declined due to dehydrogenation reactions in the plasma process, which indicated that more unsaturated products were produced with increasing the concentration of $C_{10}H_8$.

3.2 Plasma steam reforming of naphthalene

3.2.1 Influence of steam-to-carbon ratio

Steam-to-carbon ratio is a key operating parameter determining the plasma tar reforming process, as presented in Fig. 5. The destruction of naphthalene increased with increasing S/C ratio, and reached a plateau of 84.5% at a S/C of 2.0. Adding H_2O to the plasma process generates OH via the dissociation of H_2O by energetic electrons (16) and the metastable nitrogen such as $N_2(A^3\Sigma^+)$ (17), creating new reaction pathways for the further dissociation and oxidation of naphthalene and its fragments. However, upon further increasing the ratio of steam-to-carbon to 4 this substantially reduced the conversion of naphthalene. Similarly, the influence of S/C ratio on the total gas yield showed the same evolution as the conversion of naphthalene vs S/C ratio. In this study, the optimal S/C ratio was 1.5-2.0 to achieve the

highest naphthalene conversion and gas yield.

Note that the conversion of naphthalene at a larger S/C ratio of 3.0 (63.7%) and 4.0 (49.7%) was even lower than that with no steam (70.4%), suggesting the presence of excess water in the plasma process had an opposite effect on the decomposition of naphthalene. Due to the electronegative character of H_2O, electron attachment of H_2O molecules could take place and consequently reduce the density of energetic electrons (18) and the metastable nitrogen (17). Thus, the effect of water on the conversion of naphthalene has two sides and is dependent on the balance between these two opposite effects on the reaction: i) enhanced naphthalene conversion via additional oxidation routes due to the positive effect of OH radicals; and ii) reduced naphthalene conversion resulted from the negative effect of electron attachment on water (18).

$H_2O + e \rightarrow H + OH + e$ (16)

$H_2O + N_2 (A^3\Sigma^+) \rightarrow H + OH + N_2$ (17)

$H_2O + e \rightarrow H_2O^-$ (18)

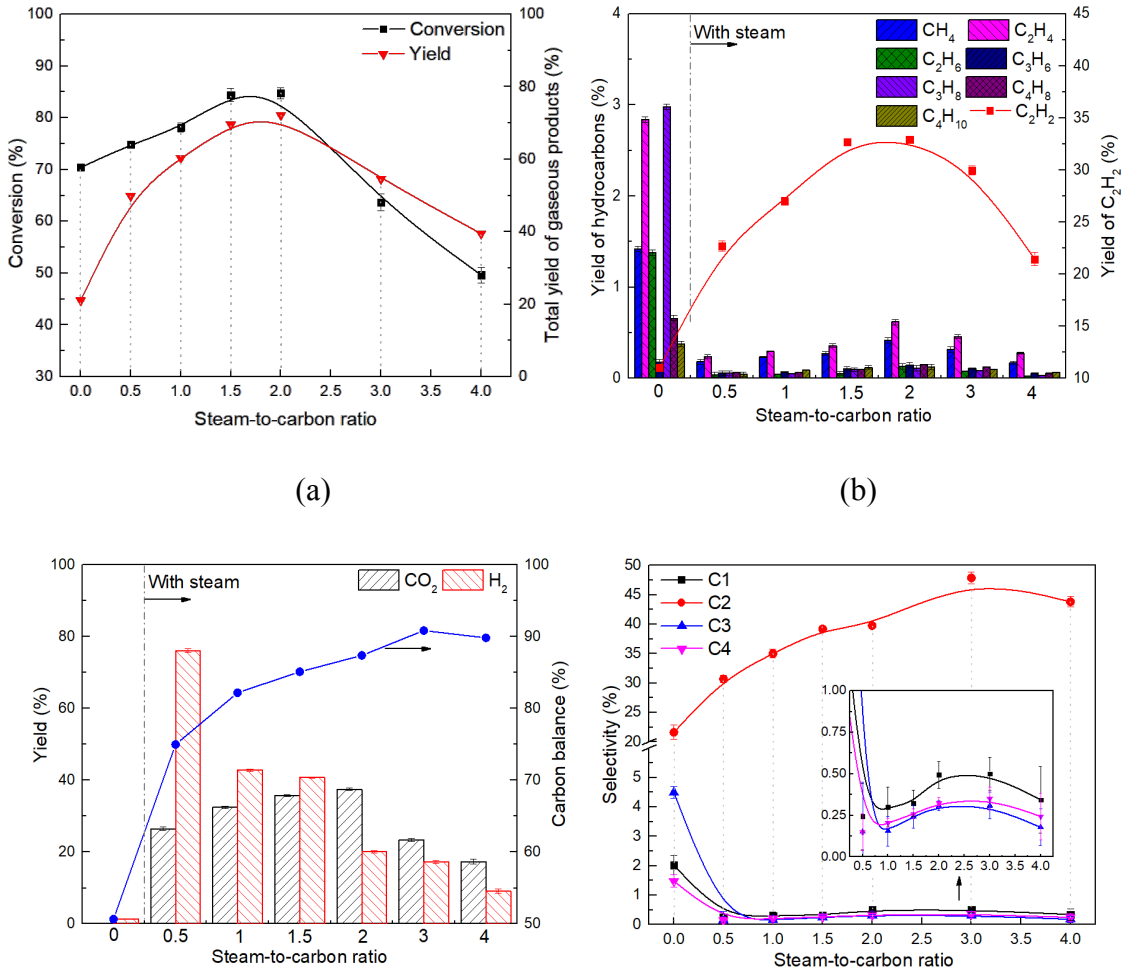

(a) (b)

(c) (d)

Fig. 5 Influence of steam-to-carbon ratio on (a) $C_{10}H_8$ conversion; (b) yield of gas products; (c) yield of CO_2 and H_2 and carbon balance; (d) selectivity of hydrocarbons with different carbon chains (C_1 – C_4) (Discharge power: 57 W; $C_{10}H_8$ content: 1.7 g/Nm^3).

In comparison to plasma reforming of naphthalene with no steam, the presence of steam in the tar reforming significantly reduced the formation of hydrocarbons except C_2H_2. The yield of C_2H_2 as a function of steam to-carbon ratio followed the same evolution as the conversion of naphthalene and total gas yield, as presented in Fig. 5(a). In addition, adding steam to this reaction produced significantly more hydrogen in comparison to the plasma processing of

naphthalene without adding steam. The highest hydrogen yield of 74.9% was obtained at a S/C ratio of 0.5, while further raising the ratio of steam-to-carbon to 4.0 dramatically decreased the hydrogen yield to 9.1% which could be attributed to the negative effect of H_2O molecules on the plasma reforming process. The yield of CO_2 increased from 26.5% to 37.5% as the S/C ratio changed from 0.5 to 2.0, and then gradually declined to 17.4% when further changing the ratio of steam-to-carbon to 4.0, thus following a similar trend to the conversion of naphthalene. It is worth noting that introducing H_2O to the plasma reduction of naphthalene process significantly reduced the carbon deposition as the carbon balance continuously increased up to 90% when varying the ratio of steam-to-carbon from 0 (without steam) to 4.0. These findings suggest that controlling appropriate steam content in the gas mixture is crucial to achieve high conversion and gas yield simultaneously in the plasma tar reforming processes, whilst keeping low carbon deposition.

Fig. 5(d) shows the influence of the steam-to-carbon ratio on the selectivity of C_1-C_4 hydrocarbons. Compared to the plasma processing of naphthalene with no steam, introducing steam to the reforming process significantly inhibited the formation of C_1, C_3 and C_4 hydrocarbons. By contrast, the selectivity of C_2 hydrocarbons increased when changing the molar ratio of steam-to-carbon from 0 to 3 and was significantly higher than that of other hydrocarbons (C_1, C_3 and C_4). Furthermore, the influence of the S/C ratio on the energy efficiency for naphthalene conversion followed a similar trend to the conversion of naphthalene and reached a peak of 5.7 g/kWh at the steam-to-carbon ratio of 1.5-2 (Fig. 6).

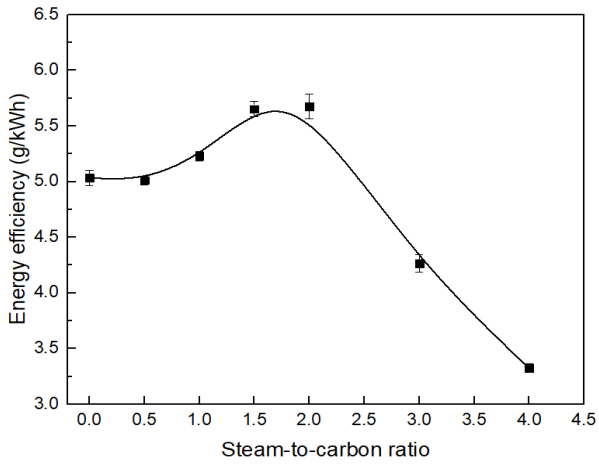

Fig. 6 Energy efficiency for $C_{10}H_8$ conversion with different S/C molar ratios ($C_{10}H_8$ content: 1.7 g/Nm^3; Discharge power: 57 W).

3.2.2 Influence of discharge power

Fig. 7 presents the influence of discharge power on the plasma steam reforming of naphthalene with the optimal molar ratio of steam-to-carbon (2.0). Increasing discharge power from 35 to 57 W notably enhanced the conversion of naphthalene by 18.2% (from 66.8% to 85%), and the total yield of gaseous products from 53.5% to 72.2%. The enhancement of the total gas yield was mainly attributed to the increased C_2H_2 yield (from 19.2% to 32.9%) when increasing the discharge power, as the yield of C_1 - C_4 hydrocarbons except C_2H_2 showed an opposite trend: decreasing with increasing discharge power, in particularly, the yield of methane dropped by around 90% from 3.5% to 0.4%.

Meanwhile, the yield of CO_2 and H_2 maintained an upward trend from 23.6% to 40.5% and from 15.4% to 25.3% respectively when increasing the discharge power, as presented in Fig. 7(c). By contrast, the CO yield declined from 5.6% (at 35 W) to 2.8% (at 51 W), and was not

detected when further increasing the discharge power to 57 W, suggesting that the water gas shift reaction (WGS) (19) could be promoted when increasing the power. This interesting finding also indicates that the discharge power could be used to control the water gas shift reaction (19) to tune the distribution of major gas products in this work.

The discharge power showed a limited effect on carbon balance which was maintained at around 88% when increasing the discharge power. This result is desirable as significantly decreased carbon balance is often found when increasing the power due to the production of more carbon in plasma reforming processes.

$$CO + H_2O \rightarrow CO_2 + H_2 \qquad (19)$$

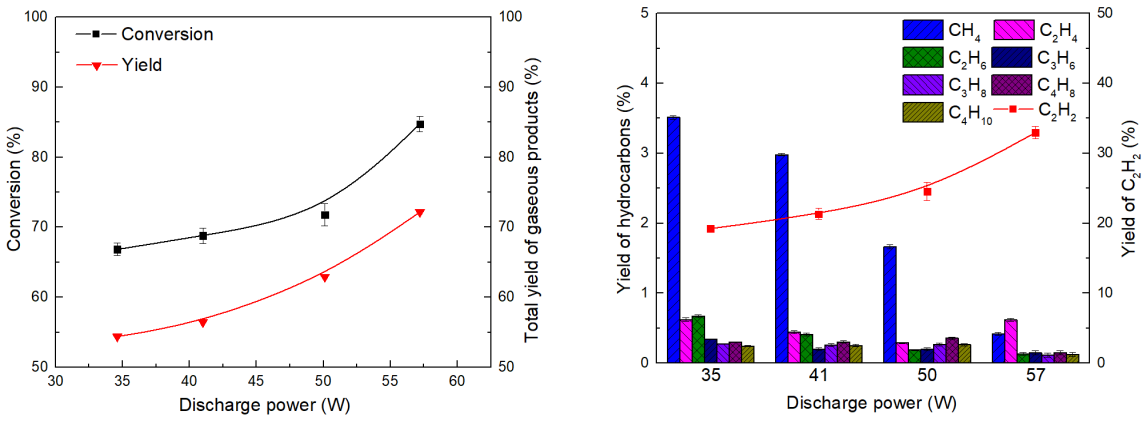

(a) (b)

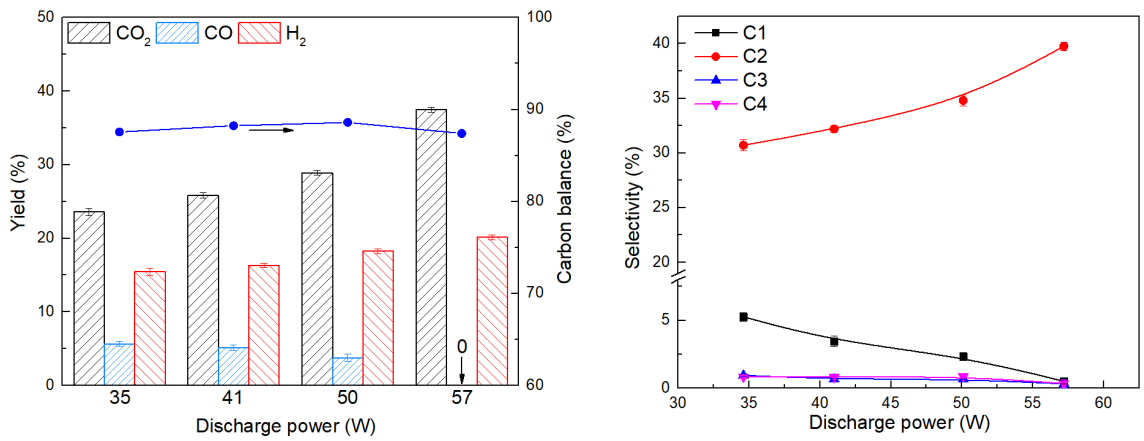

365

366 (c) (d)

367 Fig. 7 Influence of discharge power on (a) $C_{10}H_8$ conversion; (b) yield of gaseous products; (c)

368 carbon balance and yield of CO_2, CO and H_2; (d) selectivity of hydrocarbons with different

369 carbon chains (C_1 – C_4) ($C_{10}H_8$ content: 1.7 g/Nm^3; S/C ratio: 2.0).

370

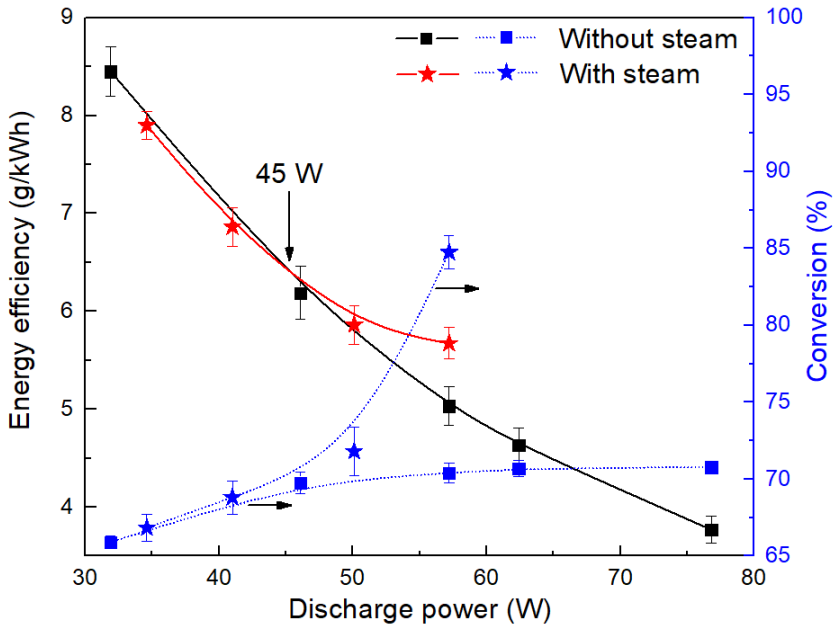

371

372 Fig. 8 Influence of plasma power and steam on the energy efficiency for the conversion of

373 naphthalene ($C_{10}H_8$ concentration: 1.7 g/Nm^3; S/C ratio: 2.0).

374

375 Fig. 8 presents the influence of steam and discharge power on the energy efficiency for the

reduction of naphthalene in the plasma tar reforming process. Clearly, the energy efficiency for naphthalene conversion decreased with an increase in discharge power regardless of the use of steam. For instance, the energy efficiency for naphthalene conversion declined from 8.4 g/kWh at 32 W to 3.5 g/kWh at 77 W. Notably, the effect of steam on the energy efficiency was limited at a lower discharge power (< 45 W). However, at a higher discharge power (> 45 W), adding steam in the plasma processing of tar enhanced the energy efficiency for naphthalene conversion in comparison to the plasma tar reforming in the absence of steam. In addition, Fig. 8 shows the presence of steam has a prominent effect on the conversion of $C_{10}H_8$ at a higher discharge power (> 45 W). Higher energy input could produce more active species (e.g. OH radicals) and electrons to compensate the negative effect of electron attachment of water (18) causing the reduced number density of reactive species (e.g., OH radicals) and electrons for tar reduction. This phenomenon reveals that choosing an appropriate plasma power is crucial to dissociate steam for the production of oxidative OH radicals as the formation of chemically reactive species and electrons in the plasma is strongly correlated to the power input.

Table 1 summarizes the performance (conversion and energy efficiency) of plasma processing of naphthalene using different non-thermal plasma processes, namely plasma oxidation of highly diluted low concentration naphthalene and plasma reforming of naphthalene with higher concentration, as limited works and data are available in the plasma reforming of naphthalene for such a comparison. Compared to the plasma reforming of naphthalene, we found that the efficiency for naphthalene conversion was higher in the

plasma oxidation of highly diluted naphthalene (20-70 ppm) using either DBD or surface discharge [22, 23]. It is important to note that the efficiency of $C_{10}H_8$ conversion is dependent on the input concentration of naphthalene, and a lower concentration of naphthalene leads to higher energy efficiency. In addition, DBD plasma is effective in the destruction of low concentration naphthalene and similarly with the oxidation of diluted VOCs. However, it is a challenge to use DBD or surface discharges for the processing of large carbon molecules such as naphthalene as a tar surrogate especially at higher concentration. This disadvantage of a DBD system is related to the relatively low electron density in DBDs and resulted polymerization taking place in the plasma destruction of naphthalene, especially in the absence of steam [26]. In addition, GAD reactors shows a stronger capacity of $C_{10}H_8$ removal at a higher concentration with an energy efficiency between 2-6 g/kWh [20]. In this work, the efficiency for the conversion of $C_{10}H_8$ was achieved at 4.6 g/kWh with a conversion of 71%, which is higher compared to previous works on the reforming of naphthalene as a tar surrogate (2.2 g/kWh). In addition, adding appropriate steam could further enhance both the conversion and efficiency to 85% and 5.7 g/kWh, respectively.

Table 1 Conversion and energy efficiency of plasma processing of naphthalene using different plasma processes.

Process	Plasma	Carrier gas	Tar [a] (g/Nm^3)	Flow rate (m^3/h)	SEI [b] (kWh/m^3)	Conversion [c] (%)	E [d] (g/kWh)	Ref
Low concentration	DBD	10% O_2/N_2	0.46	0.03	0.02	83	12.7	[23]
	Surface DBD	Air	0.37	0.03	0.02	95	17.6	[22]
	DC corona	Humid air/O_2	0.05	0.3	0.006	32	3.2	[29]
High concentration	GAD (DC) [e]	O_2	1.3	0.40	0.47	92	3.6	[20]
	GAD	C_7H_8/ Humid N_2	1.1	0.21	0.29	61	2.2	[30]
	GAD (DC) [e]	C_7H_8/ Humid N_2	7.1	4	0.1	93	62.5	[31]
	GAD	N_2	1.7	0.24	0.26	71	4.6	This work
	GAD	Humid N_2	1.7	0.24	0.25	85	5.7	This work

[a] Tar represents the initial concentration of naphthalene.

[b] SEI represents the specific energy input which is defined as the ratio of discharge power to total flow rate.

[c] Conversion represents the conversion of naphthalene.

[d] E represents the energy efficiency for naphthalene conversion.

[e] DC gliding arc plasma

3.3 Underlying mechanism for the plasma processing of naphthalene

To gain insights into the role of H_2O in the plasma naphthalene reforming, plasma spectroscopic diagnostics was carried out to better understand the production of chemically reactive species in the plasma reaction under different experimental conditions. Fig. 9(a) and

(b) show that the emission of the GAD using $N_2/C_{10}H_8$ in the absence of steam was similar to that of the $N_2/C_{10}H_8$ GAD with a low S/C (0.5). Both spectra (Fig. 9(a) and 9(b)) were dominated by the CN ($B^2\Sigma^+ \rightarrow X^2\Sigma^+$) violet system (388.3 nm, 421.6 nm) [32] and C_2 swan bands ($A^3\Pi_g \rightarrow X'^3\Pi_u$, 460 - 520 nm) [33]. Additionally, a H_γ peak ($5d^2D \rightarrow 2p^2p^0$, 433.9 nm) appeared in Fig. 9(b), and could be formed via the dissociation of H_2O (16 & 17) [25].

In the absence of steam or in the presence of limited steam (e.g., S/C=0.5), strong CN ($B^2\Sigma^+ \rightarrow X^2\Sigma$) violet bands were observed, which can be attributed to the reactions of N_2 molecules or N atoms with CH_x (x = 1 - 4) species [34, 35]. In addition, CN can also be formed through the interaction of N_2 with carbon deposition, which could explain why adding sufficient steam (e.g., S/C=4.0) to the GAD tar reforming process greatly reduces the relative emission of CN molecular bands due to less carbon deposition at a higher S/C.

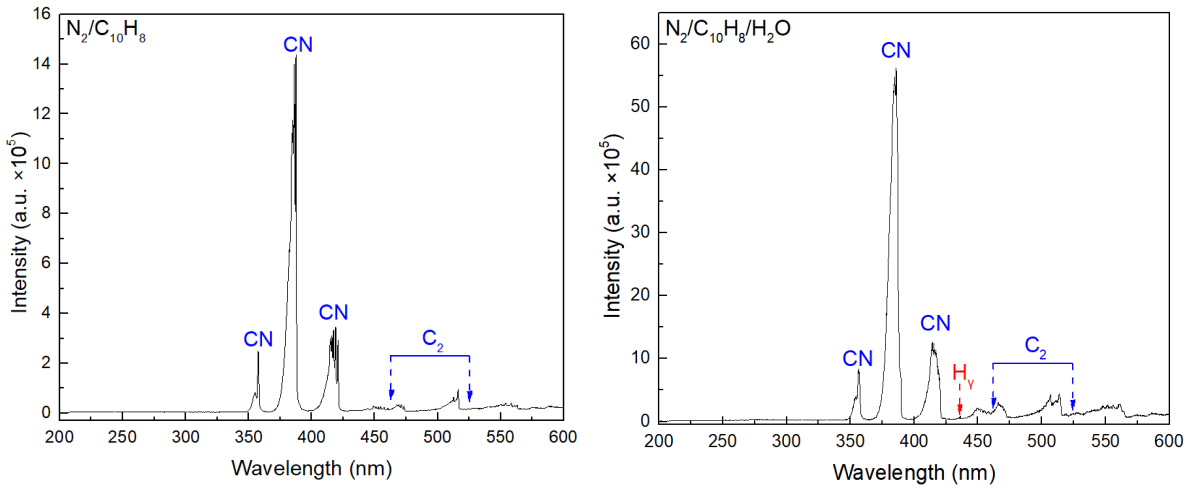

(a) (b)

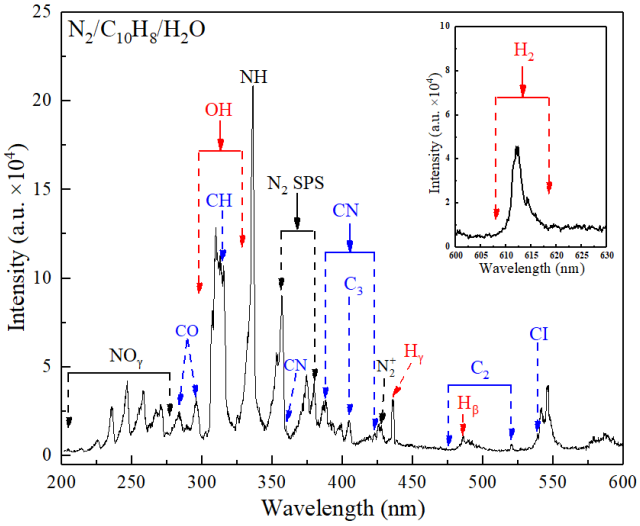

(c)

Fig. 9 Emission spectra of the GAD using (a) $N_2/C_{10}H_8$; (b) $N_2/C_{10}H_8/H_2O$ (S/C = 0.5); (c) $N_2/C_{10}H_8/H_2O$ (S/C = 2.0) ($C_{10}H_8$ content: 1.7 g/Nm^3; Discharge power: 77 W).

Compared to the plasma reforming without steam or with limited steam, Fig. 9(c) shows the presence of sufficient steam (S/C ratio = 2.0) in the nitrogen plasma reforming of naphthalene generates more reactive species. The intensity of CN molecular bands declined substantially at a higher S/C ratio (S/C ratio = 2.0) due to the generation of more oxidative species such as OH radicals, while the intensity of N_2 ($C^3\Pi_u \rightarrow B^3\Pi_g$) second positive system (357.7 nm) [36], OH ($A^2\Sigma^+ \rightarrow X^2\Pi$) bands (305 - 330 nm) and the H_γ atomic line (433.9 nm) became much stronger. In addition, H_β ($4d^2D \rightarrow 2p^2p^0$, 486.1 nm) and Fulcher-α band H_2 ($d^3\Pi_u \rightarrow a^3\Sigma_g^+$, 610 - 617 nm) were also detected, indicating the formation of hydrogen (20 and 21) [37, 38]. A strong NH ($A^2\Pi \rightarrow X^3\Sigma$) transition at 336.0 nm was found in the spectrum of the GAD with a high S/C ratio of 4.0 [39], while no NH bands were identified in the plasma reaction with a low S/C (0.5) despite more hydrogen being generated. This difference suggests that NH might not be formed directly from N_2 and H_2. By contrast, N atoms, dissociated from N_2

(22), could react with OH (23), CH_x (24), H_2 (25), and H_2O (26) species to form NH [25, 40-43]. Meanwhile, a series of carbonic species, including CO ($b^3\Sigma^+ \rightarrow a^3\Pi$, 283 nm and 297 nm) bands [42], CH ($C^2\Sigma^+ \rightarrow X^2\Pi_u$, 314.4 nm), C_3 ($A^1\Pi_u \rightarrow X^1\Sigma_g^+$, 405 nm) [43], C_2 swan system ($A^3\Pi_g \rightarrow X'^3\Pi_u$), and CI (538 nm) transition [33], were detected due to the high conversion of $C_{10}H_8$.

$$H + H + e \rightarrow H_2 + e \qquad (20)$$

$$CH_x + e \rightarrow CH_{x-2} + H_2 + e \qquad (21)$$

$$N_2 + e \rightarrow 2N + e \qquad (22)$$

$$N + OH \rightarrow NH + O \qquad k = 1.01 \times 10^{-20}\ cm^3\ molecule^{-1}\ s^{-1} \qquad (23)$$

$$N\ (^2D) + CH_4 \rightarrow NH + CH_3 \qquad k = 3.3 \times 10^{-12}\ cm^3\ molecule^{-1}\ s^{-1} \qquad (24)$$

$$N\ (^2D) + H_2 \rightarrow NH + H \qquad k = 2.3 \times 10^{-12}\ cm^3\ molecule^{-1}\ s^{-1} \qquad (25)$$

$$N\ (^2D) + H_2O \rightarrow NH + OH \qquad k = 4.2 \times 10^{-11}\ cm^3\ molecule^{-1}\ s^{-1} \qquad (26)$$

Moreover, NO_γ ($A^2\Sigma^+ \rightarrow X^2\Pi$) bands at 200-275 nm were detected when adding sufficient steam (S/C=2.0) to the plasma reforming of naphthalene [36], which suggest that NO can be formed mainly from the reaction of N_2 ($A^3\Sigma^+$) and O atom (27) [39]. Besides, N atoms could also react with OH and O_2 to form NO through the reactions (28 and 29) [39].

$$N_2\ (A^3\Sigma^+) + O \rightarrow NO\ (X^2\Pi) + N\ (^2D) \qquad (27)$$

$$N + OH \rightarrow NO + H \qquad (28)$$

$$N\ (^2D) + O_2 \rightarrow NO + O\ (^3P, {}^1D) \qquad (29)$$

To elucidate the underlying plasma chemistry and reaction pathways in the plasma processing of naphthalene, a comprehensive analysis of the condensed liquid samples was performed. The major by-products in the plasma destruction of naphthalene without steam can be classified into three groups according to their structures (Table 2): (i) unsaturated long chain hydrocarbons, including 1,5-heptadien-3-yne, 1-heptene-4-methayl, 1-hexene-4,5-dimethyl, and 3,4-isodecene; (ii) mono-substituted benzene derivatives, including toluene, benzene-1-ethynyl-4-methyl, and cyclohexane-1-ethyl-2-methyl; (iii) polycyclic hydrocarbons, including naphthalene-1,4,5,8-tetrahydro. Similar groups of by-products were also reported by Yu and his co-workers [20]. The initial destruction of naphthalene in the nitrogen GAD without steam is mainly driven by naphthalene dehydrogenation (30 and 32) and cleavage of a benzene ring (31 and 33) by electrons and metastable N_2 species such as N_2 ($A^3\Sigma^+$) [20]. However, the contribution of direct electron impact dissociation to the initial destruction of naphthalene is minor compared to metastable N_2 species which dominate the decomposition of naphthalene (30 and 31) in this process [44].

$$C_{10}H_8 + N_2^* \rightarrow C_{10}H_7 + H + N_2 \qquad (30)$$

$$C_{10}H_8 + N_2^* \rightarrow C_9H_7 + CH + N_2 \qquad (31)$$

$$C_{10}H_8 + e \rightarrow C_{10}H_7 + H + e \qquad (32)$$

$$C_{10}H_8 + e \rightarrow C_9H_7 + CH + e \qquad (33)$$

Where N_2* represents metastable nitrogen species such as N_2 (A) and N_2 (a').

Table 2 Condensed liquid by-products of plasma destruction of naphthalene with no steam

1,5-Heptadien-3-yne	1-Heptene-4-methyl
	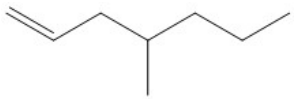
1-Hexene-4,5-dimethyl	3,4-Isodecene
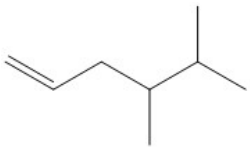	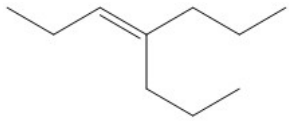
Toluene	Benzene-1-ethynyl-4-methyl
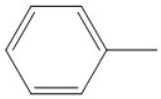	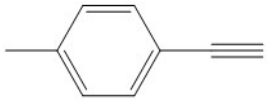
Cyclohexane-1-ethyl-2-methyl	Naphthalene-1,4,5,8-tetrahydro
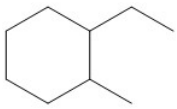	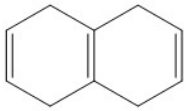

Table 3 shows that injecting H_2O to the GAD processing of naphthalene greatly minimizes the generation of by-products owing to the enhanced oxidation contributed by the presence of more oxidative species such as OH and O (34 & 35) [20, 45, 46]. The rate constant of the reaction 34 is significantly higher than that of 35, which suggests that OH radicals make a critical contribution to the plasma conversion of naphthalene.

$C_{10}H_8 + OH \rightarrow$ products $\quad k = 1 \times 10^{-11}\ cm^3\ molecule^{-1}\ s^{-1}$ (34)

$C_{10}H_8 + O \rightarrow C_{10}H_7 + OH \quad k = 3 \times 10^{-15}\ cm^3\ molecule^{-1}\ s^{-1}$ (35)

Additionally, both toluene and benzene-1-ethynyl-4-methyl were found as by-products in the

GAD processing of naphthalene regardless the use of steam. However, indene and naphthalene-1,2,3,4-tetrahydro were only found in the GAD steam reforming of naphthalene. It was reported that indene would be formed through two pathways. One is via the formation of the naphthoxy radical followed by carbon subtraction [47, 48]. The other route could be the hydrogenation and decarbonization of naphthalene [49]. In addition, naphthalene-1,2,3,4-tetrahydro could be formed through the hydrogenation of naphthalene.

Table 3 Condensed liquid by-products of plasma steam reforming of naphthalene

Toluene	Benzene-1-ethynyl-4-methyl
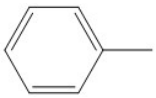	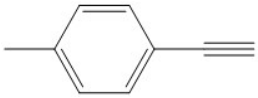
Indene	Naphthalene-1,2,3,4-tetrahydro
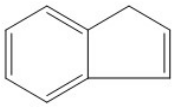	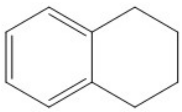

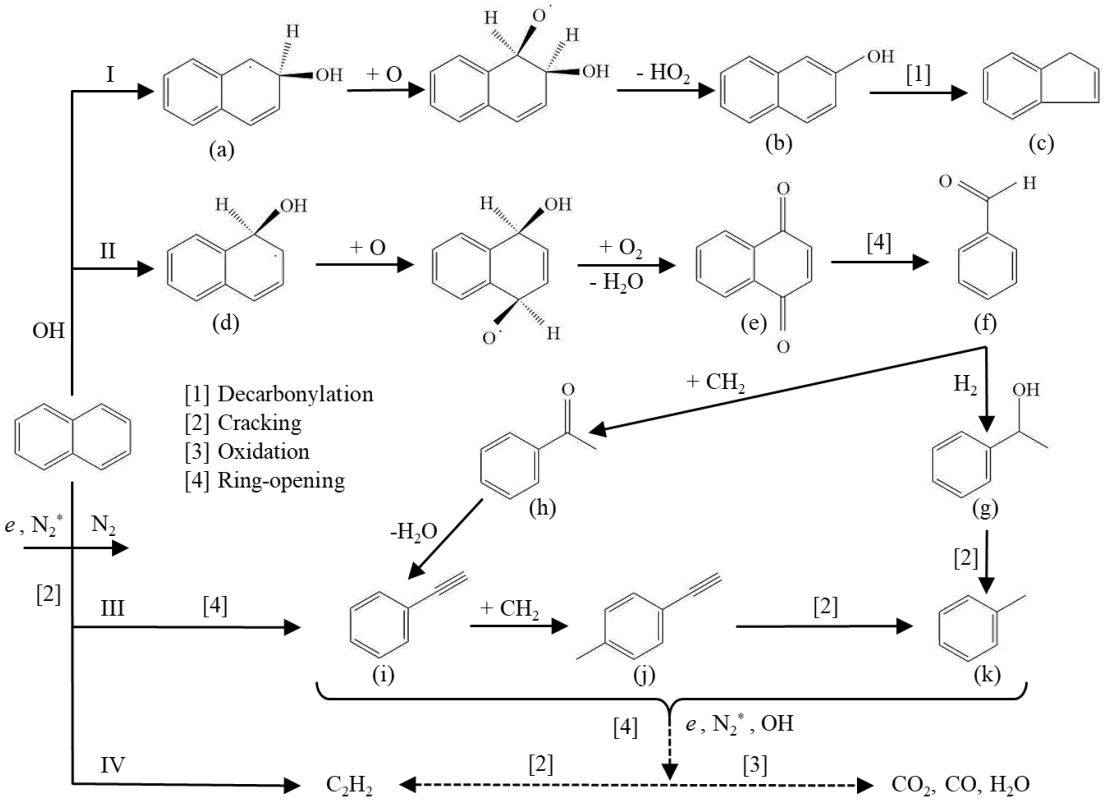

Fig. 10 Possible reaction pathways of steam reforming of naphthalene in GAD system

Fig. 10 shows the proposed reaction pathways of the GAD steam reforming of naphthalene. The OH radicals generated from H_2O dissociation in the plasma significantly contribute to the destruction of naphthalene through the recombination of an OH radical with one of the benzene rings, forming two different structures of σ-complexes ((a) and (d) in Fig. 10). Note that both σ-complexes are highly reactive as the reactions to form these σ-complexes require a negative activation energy [50]. In reaction route (I), unstable intermediates react with peroxy radicals, producing 2-naphthol (b) followed by the decarbonization of 2-naphthol to produce indene (c), one of the major by-products shown in Table 2. Meanwhile, 1,4-naphthaquinone (e) could be formed from naphthalene via the reaction route (II). The cleavage of ring in 1,4-naphthaquinone generates benzaldehyde (f), a key intermediate in this

reaction. In addition, benzyl alcohol (g) can be formed via the hydrogenation of benzaldehyde, further producing toluene (k) by cracking. On the other hand, benzaldehyde can react with CH_2 radicals to form acetophenone (h), which can be further converted to phenylethyne (i) via dehydration. Moreover, benzene-1-ethynyl-4-methyl (j) can be generated through the recombination of phenylethyne with CH_2 radicals.

In addition, the cleavage of naphthalene can take place through its collision with metastable N_2 species and energetic electrons. Route (III) shows that these ring cleavage reactions form mono-substituted benzene derivative, such as phenylethyne. Moreover, the route (IV) of $C_{10}H_8$ destruction generates C_2H_2 directly, the major gaseous product, followed by the step-wised oxidation process to form CO_2, CO and H_2O.

4. Conclusion

Plasma reforming of naphthalene as a typical two-ring tar model compound from the gasification of biomass was carried out in a GAD reactor with/without steam. The influence of key operating parameters including S/C ratio, naphthalene concentration and discharge power on the plasma processing of naphthalene was evaluated. The distribution of gaseous products could be tuned by changing these key parameters. More C_2H_2 and less CH_4 could be produced at a higher inlet concentration of naphthalene, while the highest hydrogen yield of 74.9% was obtained with the presence of limited steam (S/C=0.5) in the plasma process. An optimum S/C of 2.0 was found to obtain the highest decomposition of $C_{10}H_8$ (84.8%), C_2H_2 yield (33%), total gas yield (72.2%) and energy efficiency (5.7 g/kWh). Adding appropriate

amounts of steam to the plasma reforming of naphthalene enhanced the destruction of naphthalene, and the process efficiency whilst minimizing the generation of condensable by-products and carbon deposition. The plausible reaction routes of the plasma processing of naphthalene were proposed through a comprehensive analysis of gaseous and condensable products combined with optical emission spectroscopic diagnostics. Naphthalene dehydrogenation and cleavage of benzene ring have been identified as the two major reactions for the initial decomposition of naphthalene. Dissociation of naphthalene by metastable nitrogen species dominates the destruction of naphthalene, while direct electron impact dissociation makes a minor contribution to the decomposition of naphthalene. The generated OH radicals initiate step-wised oxidation of naphthalene and its fragments towards to the formation of CO, CO_2 and water.

Acknowledgements

The authors would like to thank for the financial support from the EPSRC Impact Acceleration Account (IAA), the Royal Society Newton Advanced Fellowship (Ref. NAF/R1/180230) and the Foundation of State Key Laboratory of Coal Combustion at HUST (No. FSKLCCB1805). We acknowledge the European Union (EU) and Horizon 2020 funding awarded under the Marie Sklodowska-Curie Action to the EUROPAH Consortium (Grant Number 722346).

References

[1] Z. Zhang, L. Liu, Preparation, modification and development of Ni-based catalysts for catalytic reforming of tar produced from biomass gasification, Renew. Sustain. Energy Rev. 94 (2018) 1086–1109. doi:10.1016/j.rser.2018.07.010.

[2] S. Anis, Z.A. Zainal, Tar reduction in biomass producer gas via mechanical, catalytic and thermal methods: A review, Renew. Sustain. Energy Rev. 15 (2011) 2355–2377. doi:10.1016/j.rser.2011.02.018.

[3] Y. Richardson, J. Blin, A. Julbe, A short overview on purification and conditioning of syngas produced by biomass gasification: Catalytic strategies, process intensification and new concepts, Prog. Energy Combust. Sci. 38 (2012) 765–781. doi:10.1016/j.pecs.2011.12.001.

[4] B.S. Pathak, D. V. Kapatel, P.R. Bhoi, A.M. Sharma, D.K. Vyas, Design and development of sand bed filter for upgrading producer gas to IC engine quality fuel, Int. Energy J. 8 (2007) 15–20.

[5] L. Fagbemi, L. Khezami, R. Capart, Pyrolysis products from different biomasses: application to the thermal cracking of tar, Appl. Energy. 69 (2001) 293–306. doi:10.1016/S0306-2619(01)00013-7.

[6] Z. Min, P. Yimsiri, S. Zhang, Y. Wang, M. Asadullah, C.Z. Li, Catalytic reforming of tar during gasification. Part III. Effects of feedstock on tar reforming using ilmenite as a catalyst, Fuel. 103 (2013) 950–955. doi:10.1016/j.fuel.2012.09.019.

[7] N. Gao, X. Wang, A. Li, C. Wu, Z. Yin, Hydrogen production from catalytic steam reforming of benzene as tar model compound of biomass gasification, Fuel Process.

Technol. 148 (2016) 380–387. doi:10.1016/j.fuproc.2016.03.019.

[8] J. Han, H. Kim, The reduction and control technology of tar during biomass gasification/pyrolysis: An overview, Renew. Sustain. Energy Rev. 12 (2008) 397–416. doi:10.1016/j.rser.2006.07.015.

[9] L. Wang, Y. Yi, C. Wu, H. Guo, X. Tu, One-Step Reforming of CO2and CH4into High-Value Liquid Chemicals and Fuels at Room Temperature by Plasma-Driven Catalysis, Angew. Chemie - Int. Ed. 56 (2017) 13679–13683. doi:10.1002/anie.201707131.

[10] L. Wang, Y. Yi, H. Guo, X. Tu, Atmospheric Pressure and Room Temperature Synthesis of Methanol through Plasma-Catalytic Hydrogenation of CO2, ACS Catal. 8 (2018) 90–100. doi:10.1021/acscatal.7b02733.

[11] A.H. Khoja, M. Tahir, N.A.S. Amin, Recent developments in non-thermal catalytic DBD plasma reactor for dry reforming of methane, Energy Convers. Manag. 183 (2019) 529–560. doi:10.1016/j.enconman.2018.12.112.

[12] L. Li, H. Zhang, X. Li, X. Kong, R. Xu, K. Tay, X. Tu, Plasma-assisted CO2 conversion in a gliding arc discharge: Improving performance by optimizing the reactor design, J. CO2 Util. 29 (2019) 296–303. doi:10.1016/j.jcou.2018.12.019.

[13] C.M. Du, J.H. Yan, B. Cheron, Decomposition of toluene in a gliding arc discharge plasma reactor, Plasma Sources Sci. Technol. 16 (2007) 791–797. doi:10.1088/0963-0252/16/4/014.

[14] L. Liu, Q. Wang, S. Ahmad, X. Yang, M. Ji, Y. Sun, Steam reforming of toluene as model biomass tar to H2-rich syngas in a DBD plasma-catalytic system, J. Energy Inst.

91 (2018) 927–939. doi:10.1016/j.joei.2017.09.003.

[15] L. Mao, Z. Chen, X. Wu, X. Tang, S. Yao, X. Zhang, B. Jiang, J. Han, Z. Wu, H. Lu, T. Nozaki, Plasma-catalyst hybrid reactor with CeO2/Γ-Al2O3for benzene decomposition with synergetic effect and nano particle by-product reduction, J. Hazard. Mater. 347 (2018) 150–159. doi:10.1016/j.jhazmat.2017.12.064.

[16] A.A. Najafpoor, A. Jonidi Jafari, A. Hosseinzadeh, R. Khani Jazani, H. Bargozin, Optimization of non-thermal plasma efficiency in the simultaneous elimination of benzene, toluene, ethyl-benzene, and xylene from polluted airstreams using response surface methodology, Environ. Sci. Pollut. Res. 25 (2018) 233–241. doi:10.1007/s11356-017-0373-8.

[17] J. Gao, Y. Liu, W. Yang, L. Pu, J. Yu, Q. Lu, Oxidative degradation of phenol in aqueous electrolyte induced by plasma from a direct glow discharge, Plasma Sources Sci. Technol. 12 (2003) 533–538. doi:10.1088/0963-0252/12/4/305.

[18] Y.C. Yang, Y.N. Chun, Naphthalene destruction performance from tar model compound using a gliding arc plasma reformer, Korean J. Chem. Eng. 28 (2011) 539–543. doi:10.1007/s11814-010-0393-2.

[19] J. Yan, X. Li, X. Tu, F. Zhu, H. Zhang, R. Xu, L. Li, Steam reforming of toluene and naphthalene as tar surrogate in a gliding arc discharge reactor, J. Hazard. Mater. 369 (2019) 244–253. doi:10.1016/j.jhazmat.2019.01.085.

[20] L. Yu, X. Li, X. Tu, Y. Wang, S. Lu, J. Yan, Decomposition of naphthalene by dc gliding arc gas discharge, J. Phys. Chem. A. 114 (2010) 360–368. doi:10.1021/jp905082s.

[21] A.A. Abdelaziz, T. Seto, M. Abdel-Salam, Y. Otani, Influence of N2/O2mixtures on decomposition of naphthalene in surface dielectric barrier discharge based reactor, Plasma Chem. Plasma Process. 34 (2014) 1371–1385. doi:10.1007/s11090-014-9578-5.

[22] A.A. Abdelaziz, T. Seto, M. Abdel-Salam, Y. Otani, Performance of a surface dielectric barrier discharge based reactor for destruction of naphthalene in an air stream, J. Phys. D. Appl. Phys. 45 (2012) 115201 (10pp). doi:10.1088/0022-3727/45/11/115201.

[23] Z. Wu, J. Wang, J. Han, S. Yao, S. Xu, P. Martin, Naphthalene Decomposition by Dielectric Barrier Discharges at Atmospheric Pressure, IEEE Trans. Plasma Sci. 45 (2017) 154–161. doi:10.1109/TPS.2016.2632154.

[24] Z. Wu, Z. Zhu, X. Hao, W. Zhou, J. Han, X. Tang, S. Yao, X. Zhang, Enhanced oxidation of naphthalene using plasma activation of TiO2/diatomite catalyst, J. Hazard. Mater. 347 (2018) 48–57.

[25] S. Liu, D. Mei, L. Wang, X. Tu, Steam reforming of toluene as biomass tar model compound in a gliding arc discharge reactor, Chem. Eng. J. 307 (2017) 793–802. doi:10.1016/j.cej.2016.08.005.

[26] X. Tu, J.C. Whitehead, ScienceDirect Plasma dry reforming of methane in an atmospheric pressure AC gliding arc discharge : Co- generation of syngas and carbon nanomaterials, Int. J. Hydrogen Energy. 39 (2014) 9658–9669. doi:10.1016/j.ijhydene.2014.04.073.

[27] F. Zhu, X. Li, H. Zhang, A. Wu, J. Yan, M. Ni, H. Zhang, A. Buekens, Destruction of

toluene by rotating gliding arc discharge, Fuel. 176 (2016) 78–85. doi:10.1016/j.fuel.2016.02.065.

[28] P. Jamróz, W. Kordylewski, M. Wnukowski, Microwave plasma application in decomposition and steam reforming of model tar compounds, Fuel Process. Technol. 169 (2018) 1–14. doi:10.1016/j.fuproc.2017.09.009.

[29] M. Ni, X. Shen, X. Gao, Z. Wu, H. Lu, Z. Li, Z. Luo, K. Cen, Naphthalene decomposition in a DC corona radical shower discharge, J. Zhejiang Univ. Sci. A. 12 (2011) 71–77. doi:10.1631/jzus.A1010009.

[30] S. Liu, Plamsa gas cleaning Processes for the conversion of model tar from biomass gasification, University of Liverpool, 2017.

[31] T. Nunnally, A. Tsangaris, A. Rabinovich, G. Nirenberg, I. Chernets, A. Fridman, Gliding arc plasma oxidative steam reforming of a simulated syngas containing naphthalene and toluene, Int. J. Hydrogen Energy. 39 (2014) 11976–11989. doi:10.1016/j.ijhydene.2014.06.005.

[32] K.J. Clay, S.P. Speakman, G.A.J. Amaratunga, S.R.P. Silva, Characterization of a-C:H:N deposition from CH4/N2rf plasmas using optical emission spectroscopy, J. Appl. Phys. 79 (1996) 7227–7233. doi:10.1063/1.361439.

[33] H.H. Mi, W.T. Liao, H.C. Chang, S.J. Chen, C.C. Lin, L. Te Hsieh, Optical emission spectroscopy in cooking exhaust from a wet scrubber/atmospheric plasma reactor, Aerosol Air Qual. Res. 14 (2014) 1665–1674. doi:10.4209/aaqr.2014.01.0002.

[34] C.D. Pintassilgo, C. Jaoul, J. Loureiro, T. Belmonte, T. Czerwiec, Kinetic modelling of a N2 flowing microwave discharge with CH4 addition in the post-discharge for

nitrocarburizing treatments, J. Phys. D. Appl. Phys. 40 (2007) 3620–3632. doi:10.1088/0022-3727/40/12/011.

[35] H. Zhang, C. Du, A. Wu, Z. Bo, J. Yan, X. Li, Rotating gliding arc assisted methane decomposition in nitrogen for hydrogen production, Int. J. Hydrogen Energy. 39 (2014) 12620–12635. doi:10.1016/j.ijhydene.2014.06.047.

[36] D. Xiao, C. Cheng, J. Shen, Y. Lan, H. Xie, X. Shu, Y. Meng, J. Li, P.K. Chu, Characteristics of atmospheric-pressure non-thermal N2and N2/O2gas mixture plasma jet, J. Appl. Phys. 115 (2014) 1–10. doi:10.1063/1.4862304.

[37] T. Shikama, S. Kado, Y. Kuwahara, K. Kurihara, F. Scotti, S. Tanaka, Fulcher-α Band Spectra in Mixed Hydrogen Isotope Plasmas, Plasma Fusion Res. 2 (2007) S1045. doi:10.1585/pfr.2.S1045.

[38] M. Goujon, T. Belmonte, G. Henrion, OES and FTIR diagnostics of HMDSO/O2SiOxdeposition assisted by RF plasma, Surf. Coatings Technol. 188–189 (2004) 756–761. doi:10.1016/j.surfcoat.2004.07.048.

[39] H. Zhang, F. Zhu, X. Li, K. Cen, C. Du, X. Tu, Rotating Gliding Arc Assisted Water Splitting in Atmospheric Nitrogen, Plasma Chem. Plasma Process. 36 (2016) 813–834. doi:10.1007/s11090-016-9700-y.

[40] T. Verreycken, P.J. Bruggeman, OH density measurements in nanosecond pulsed discharges in atmospheric pressure N2-H2O mixtures, Plasma Sources Sci. Technol. 23 (2014). doi:10.1088/0963-0252/23/1/015009.

[41] J.T. Herron, Evaluated chemical kinetics data for reactions of N(2D), N(2P), and N2(A3Σ+u) in the gas phase, J. Phys. Chem. Ref. Data. 28 (1999) 1453–1483.

doi:10.1063/1.556043.

[42] M. Kraus, W. Egli, K. Haffner, B. Eliasson, U. Kogelschatz, A. Wokaun, Investigation of mechanistic aspects of the catalytic CO2 reforming of methane in a dielectric-barrier discharge using optical emission spectroscopy and kinetic modeling, Phys. Chem. Chem. Phys. 4 (2002) 668–675. doi:10.1039/b108040g.

[43] J. Luque, W. Juchmann, E.A. Brinkman, J.B. Jeffries, Excited state density distributions of H, C, C2, and CH by spatially resolved optical emission in a diamond depositing dc-arcjet reactor, J. Vac. Sci. Technol. A Vacuum, Surfaces, Film. 16 (1998) 397–408. doi:10.1116/1.581037.

[44] A.N. Trushkin, M.E. Grushin, I. V. Kochetov, N.I. Trushkin, Y.S. Akishev, Decomposition of toluene in a steady-state atmospheric-pressure glow discharge, Plasma Phys. Reports. 39 (2013) 167–182. doi:10.1134/S1063780X13020025.

[45] R. Atkinson, S.M. Aschmann, Kinetics of the reactions of naphthalene, 2-methylnaphthalene, and 2,3-dimethylnaphthalene with OH radicals and with O3 at 295 ± 1 K, Int. J. Chem. Kinet. 18 (1986) 569–573. doi:10.1002/kin.550180507.

[46] R. Atkinson, Kinetics and mechanisms of the gas-phase reactions of the hydroxyl radical with organic compounds under atmospheric conditions, Chem. Rev. 86 (1986) 69–201. doi:10.1021/cr00071a004.

[47] L. Devi, K.J. Ptasinski, F.J.J.G. Janssen, Decomposition of naphthalene as a biomass tar over pretreated olivine: Effect of gas composition, kinetic approach, and reaction scheme, Ind. Eng. Chem. Res. 44 (2005) 9096–9104. doi:10.1021/ie050801g.

[48] N.M. MARINOV, M.J. CASTALDI, C.F. MELIUS, W. TSANG, Aromatic and

Polycyclic Aromatic Hydrocarbon Formation in a Premixed Propane Flame, Combust. Sci. Technol. 128 (1997) 295–342. doi:10.1080/00102209708935714.

[49] W.D. Gräber, K.J. Hüttinger, Chemistry of methane formation in hydrogasification of aromatics. 1. Non-substituted aromatics, Fuel. 61 (1982) 499–504. doi:10.1016/0016-2361(82)90170-3.

[50] H.W. Biermann, H. Mac Leod, A.M. Winer, J.N. Pitts, R. Atkinson, Kinetics of the Gas-Phase Reactions of the Hydroxyl Radical with Naphthalene, Phenanthrene, and Anthracene, Environ. Sci. Technol. 19 (1985) 244–248. doi:10.1021/es00133a004.